The influence of chemical surface patterning on the freezing behaviour of impacting supercooled water droplets

Tavaststjerna, M. J.; Ding, M.; Hussong, J.; Picken, S. J.; Roisman, I. V.; Garcia, S. J.

DOI
10.1016/j.surfin.2025.107918

Publication date
2025

Document Version
Final published version

Published in
Surfaces and Interfaces

Surfaces and Interfaces 76 (2025) 107918

Contents lists available at ScienceDirect

Surfaces and Interfaces

journal homepage: www.sciencedirect.com/journal/surfaces-and-interfaces

The influence of chemical surface patterning on the freezing behaviour of impacting supercooled water droplets

M.J. Tavaststjerna [a,1], M. Ding [b,1], J. Hussong [b], S.J. Picken [c], I.V. Roisman [b], S.J. Garcia [a,*]

[a] Department of Aerospace Structures and Materials, Faculty of Aerospace Engineering, Delft University of Technology, Kluyverweg 1, 2629 HS Delft, the Netherlands
[b] Institute for Fluid Mechanics and Aerodynamics, Technical University of Darmstadt, Peter-Grünberg-Straße 10, 64287 Darmstadt, Germany
[c] Department of Chemical Engineering, Faculty of Applied Sciences, Delft University of Technology, Van der Maasweg 9, 2629 HZ Delft, the Netherlands

ARTICLE INFO

Keywords:
Aircraft icing
Anti-icing
Supercooled droplet
Impact icing
Patterned wettability
Droplet impact

ABSTRACT

Impacting supercooled water droplets commonly cause in-flight ice accumulation on aircraft surfaces. Ice accretion can lead to dangerous situations such as disturbance of airflow around the aircraft wings, breakdown of vital antennae, or even malfunction of the engines. The adverse effects of aircraft icing could be avoided by designing passive anti-icing surfaces that either delay ice nucleation after droplet impact and/or reduce ice adhesion to promote its shedding. Among potential passive anti-icing strategies, smooth surfaces with patterned hydrophilic and hydrophobic regions have shown good potential to control local frost formation. In this study, we investigate how hydrophilic 150 μm wide stripes influence the impact and freezing of supercooled water droplets on two polymeric substrates (Polyvinylchloride and Polypropylene). In addition to varying the wettability difference between the stripes and the substrate, the distance between the stripes (1.25—10 mm) and the impact velocity of the water droplet (4.1—6.5 m/s) were varied. High-speed video analysis of the impacting droplets shows that the presence of the hydrophilic patterns can lower ice nucleation rates and direct the shape of the droplet spreading after impact. However, a low wettability difference between the substrate and the patterns can lead to the opposite scenario with higher nucleation rates.

1. Introduction

Due to significant safety hazards and increased fuel consumption, ice accretion on aircraft wings, engines, and antennae is a substantial concern for aviation [1–3]. Currently, in-flight ice accretion is managed using various active de-icing methods that rely on external energy, including thermal protection through heating wing surfaces, chemical protection by spraying the surfaces with de-icing fluids, or mechanical protection by attaching inflatable pneumatic boots onto the wings. Since these active methods increase energy consumption and add weight to the aircraft, an alternative strategy could be to create passive anti-icing coatings that inherently delay ice nucleation and/or reduce ice adhesion, thus promoting its shedding [3–6]. The most researched passive anti-icing strategies rely on water-repelling superhydrophobic surfaces or slippery liquid-infused surfaces, while concepts combining stiffness and chemical patterning are gaining attention.

Although some passive anti/low icing technologies effectively reduce condensation frosting and ice adhesion strength, their performance in dynamic icing conditions, more relevant from the in-flight perspective, requires further research. The case of supercooled impact droplets is even less studied due to its complexity. When an aircraft passes through cold cloud formations, supercooled water droplets within the clouds impact the aircraft's surface at high velocities. In the particular case of water-repelling superhydrophobic surfaces and slippery liquid-infused surfaces, the impacting water droplets freeze quickly upon impact and generate fast-growing layers of ice that mechanically interlock with the rough superhydrophobic surface structures, leading to higher ice adhesion or wear out the lubricating liquids from the surface, hence reducing the long-term efficiency [7–12].

Alternatively, surfaces combining hydrophilic and hydrophobic regions have shown some success in controlling static frost propagation and condensation in high and low supersaturation conditions [13–15]. These patterned wettability surfaces have also attracted interest for applications related to dynamic icing conditions with the aim of controlling where and what type of ice forms on the aircraft's surface [4,16,17]. However, to construct a rational design for a chemically patterned

* Corresponding author.
E-mail address: s.j.garciaespallargas@tudelft.nl (S.J. Garcia).
[1] These authors contributed equally to this work

https://doi.org/10.1016/j.surfin.2025.107918
Received 14 July 2025; Received in revised form 20 September 2025; Accepted 18 October 2025
Available online 22 October 2025

anti-icing coating, it is imperative to understand the physics of supercooled water droplet impact on uniform and patterned surfaces, an aspect so far not investigated.

The state-of-the-art in supercooled droplet impact studies make use of high-speed imaging and the interpretation of the videos through thermodynamics and hydrodynamics to study the mechanisms involved in the impact and solidification of supercooled water droplets [18–21]. Once a supercooled water droplet impacts a smooth surface, the droplet spreads and then recedes, forming a thin film over the surface. During this process, air bubbles can become entrapped within the film, introducing localized instabilities in the liquid and creating favourable conditions for ice nucleation and subsequent solidification [20].

Since nucleation events in the film are stochastic, multiple experiments of the same sample under the same conditions must be analysed to understand the droplet freezing behaviour. To compare the freezing behaviour of different samples in different environments quantitatively, a statistical model [22] can be used to derive the rate of heterogeneous nucleation per unit area $J_s(t)$. During video analysis, the droplet freezing onset time is recorded individually for each experiment. For each recorded freezing onset time (t), the average number of nucleation sites per unit area at time t, $\lambda_s(t)$, can be estimated by [20,22]

$$\lambda_s(t) = \frac{1}{A_c(t)} \ln\left(\frac{N_0}{N_{liq}(t)}\right) \equiv \int_0^t J_s dt \quad (1)$$

where $A_c(t)$ is the wetted surface area of the droplet at freezing onset time (t), $N_{liq}(t)$ is the number of experiments where the freezing onset time is higher than time (t), and N_0 is the overall number of experiments. Even though this statistical model has been used to compare droplet nucleation rates on various uniform aluminium and superhydrophobic surfaces in different environmental conditions [20,22,23] it has not yet been applied to patterned wettability surfaces.

So far, only a few studies have investigated the dynamic behaviour of impacting water droplets on patterned wettability surfaces [24–29]. However, these studies rely on computational modelling and focus on droplet impact and wetting in a room temperature environment, instead of supercooled conditions. One of these simulates the impact of glycerol droplets (diameter $D_0 = 2.45$ mm and impact velocity 0.2 m/$s \leq U_0 \leq 2$ m/s) on hydrophobic surfaces (static water contact angle WCA∼95°) patterned with four hydrophilic squares (WCA∼15°) using an immersed boundary-based framework [25]. The results show how the droplet breaks into four sections at impact, followed by selective wetting of the four hydrophilic areas. Although this work focuses on glycerol droplets at room temperature conditions, it demonstrates the ability of hydrophilic patterning to influence the shape of the thin film after droplet impact by sufficient dewetting at the hydrophobic substrate combined with easy wetting of the hydrophilic square patterns.

A similar study models the impact of water droplets (diameter $D_0 =$ 0.025 mm) on hydrophilic glass (WCA∼45°) patterned with cross-shaped or inverted cross-shaped hydrophobic areas (WCA∼120°) using a multiphase lattice Boltzmann method [24]. This simulation also showed the water droplet splitting and transporting toward the hydrophilic regions, with experimental results supporting the numerical models. While the impacting water droplets have been shown to deform, split, and spread according to the hydrophilic pattern design in ambient conditions, the ability of the patterning to influence dynamic droplet freezing behaviour is yet unknown. Potentially, patterned wettability surfaces could help direct the freezing of impacting droplets to a specific shape or spatial distribution in dynamic icing conditions, which may help to reduce airflow disruption around aircraft wings or simply lower the ice adhesion or facilitate ice separation.

So far, the influence of wettability patterns on droplet impact has promising computational results; however, only a few experimental studies support these numerical models. Furthermore, neither numerical simulations nor experimental studies have been reported for droplet impact on patterned wettability surfaces in cooled or supercooled conditions. Although patterned wettability surfaces have already been suggested as a solution for impact icing conditions, the literature lacks any systematic experimental evidence to support this proposition. This work presents the first systematic investigation of the influence of patterned wettability on supercooled water droplet impact, wetting, and freezing behavior on surfaces. The supercooled droplet impact experiments were carried out with three different impact velocities on polymeric substrates patterned with hydrophilic stripes. Two types of commodity polymers (PP and PVC) were functionalized with hydrophilic poly(2-hydroxyethyl methacrylate) (PHEMA) brushes to prepare the patterned samples. Samples with varying numbers of hydrophilic stripes were used to examine the influence of stripe-to-stripe distance on the dynamic droplet impact behaviour. The droplet impact, wetting, and freezing dynamics are here related to the substrate type, hydrophilic stripe distance, and droplet impact velocity using high-speed camera imaging and statistical analysis of the high-speed videos.

2. Experimental

2.1. Sample preparation

The polymeric substrates PP and PVC (20 × 20 × 1 mm) used in this work were purchased from S-Polytec GmbH, and were functionalized with poly(2-hydroxyethyl methacrylate) (PHEMA) grafted with the help of bifunctional macroinitiator PAzBrMA as reported elsewhere [15]. To create the stripes, UV masks with constant stripe width of 150 μm and varying stripe distances of 1.2 mm, 2.5 mm, 5 mm, and 10 mm were used to allow covalently fixing the macroinitiator only at stripe locations on the PVC and PP substrates upon exposure to a UV lamp (OmniCure S2000 UV Curing System, 320–500 nm) with 30 W/cm^2 for 5 min. This was followed by rinsing to remove the unreacted PAzBrMA, exposure to PHEMA for reaction with the macroinitiator at the stripe locations, and rinsing again to remove the excess PHEMA. The resulting samples are polymeric substrates (PP or PVC) patterned with hydrophilic polymer brushes (PHEMA), which are covalently anchored to the substrate surface.

2.2. Water contact angle measurements

Water contact angles (WCA) of the bare and grafted polymer surfaces were determined using a KSV CAM 200 optical contact angle goniometer. Static, advancing, and receding contact angles were recorded using the sessile and needle-in-the-sessile-droplet methods. All measurements were repeated three times for each sample. For advancing and receding contact angles, the initial volume of the droplet (3 μL) was first increased with a pumping speed of 15 μL/s until a maximum droplet size of 15 μL. Then, the volume of the droplet was decreased from 15 μL back to 3 μL using the same pumping speed of 15 μL/s. All contact angle measurements were carried out at an ambient temperature of 21 $^\circ C \pm 2$ and relative humidity of 40 % ±5.

2.3. Surface imaging

The polymeric substrates were imaged before and after the surface functionalization using Laser Scanning Confocal Microscopy (Keyence VK-X1000) and micro-FTIR (PerkinElmer Spotlight 400). The 3D Laser Scanning Confocal images were further analysed to determine area roughness values (Sa) for the sample surfaces.

2.4. Supercooled water droplet impact test

The droplet impact tests were conducted inside an l-shaped wind tunnel in isothermal conditions (−10 °C) with airflow set to vary between 0, 10, and 20 m/s. A schematic presentation of the experimental setup for investigating supercooled droplet impact on the patterned

surfaces is presented in Fig. 1. The supercooled droplet was generated with a syringe needle on top of the wind tunnel, from where the droplet was directed to fall on top of the sample substrate placed at the test section of the vertical wind tunnel. To ensure that the impacting droplets were in a supercooled state, a thin thermocouple was kept inside the needle to monitor the droplet temperature during the experiments. Additionally, the samples were kept inside the wind tunnel for a minimum of 30 min before each experiment to cool them down to the desired surface temperature of −10 °C. The droplet impact onto the sample surface was recorded with a high-speed camera (Photron SA-X2 k1080, 8000 fps, 52.91 μm/pixel). Since the droplet impact was imaged at an angle of 40°, a calibration algorithm was used to calculate distances during image processing. The droplet impact tests were repeated a minimum of 10 times for each sample per air flow condition. A detailed description of the experimental setup is provided elsewhere [20].

3. Results and discussion

3.1. Sample preparation

Two commodity polymeric substrates (PP and PVC) were functionalized with hydrophilic poly(2-hydroxyethyl methacrylate) (PHEMA) stripes to investigate supercooled droplet impact on patterned wettability surfaces. To ensure the durability of the patterning during repeated droplet impact tests on the same location, the hydrophilic PHEMA polymer was covalently linked to the substrates via a bifunctional macroinitiator PAzBrMA [15]. The azide functionalities of PAzBrMA enabled the covalent attachment of the macroinitiator to the substrate under UV light exposure, while the remaining bromide functionalities act as initiation points for surface-initiated atom transfer radical polymerization (SI-ATRP) of hydrophilic monomer HEMA.

To create the patterns, UV masks cut with 100 μm thin slits were placed on top of the substrates covered with PAzBrMA. Upon UV exposure, the PAzBrMA located at the areas where the slit is located becomes covalently bound to the surface, while the unreacted PAzBrMA chains beyond the slit openings can be rinsed away. This is followed by exposure to HEMA to polymerize where the fixed PAzBrMA is located (i.e., at the stripes). The distance between the stripes was varied from 1.25 mm to 10 mm by changing the design of the UV mask. As a result, 10 different types of samples: bare PP and PVC substrates with no stripes and PP and PVC patterned with a stripe distribution of 1.2 mm, 2.5 mm, 5 mm, and 10 mm.

As shown in Fig. 2, PP shows about two times higher roughness (1.50 μm > 0.8 μm), slightly higher static water contact angle (101° > 96°) and lower contact angle hysteresis (30° < 59°) than is the case for PVC.

Confocal imaging and micro-FTIR confirmed fixation, stripe size, conformality, and roughness of the PHEMA patterns. The hydrophilic polymer brushes should be thin enough to avoid significantly changing the roughness of the sample surface, which could interfere with the droplet spreading behaviour and freezing probability. As seen in Figs. 2 and **S1**, the width of the stripes is approximately 150 μm, and the thickness is lower than 0.3 μm after 4 h of polymerization in HEMA solutions. Analysis of samples fully covered with PHEMA (without a mask during UV exposure) showed that the surface functionalization did not influence the overall roughness of the substrates. In contrast, the wettability of the PHEMA-covered areas was lowered to a static water contact angle of 41° (from initial 101° and 96° of PP and PVC, respectively).

3.2. Influence of hydrophilic patterns on droplet impact

Supercooled droplet impact on the patterned surfaces was investigated in an l-shaped wind tunnel built inside a cold chamber (see Fig. 1). Before each experiment, the sample was attached to a round sample stage positioned in the middle of the wind tunnel. The temperature inside the cold chamber was set to −10 °C, and the airflow inside the wind tunnel was varied between 0, 10, and 20 m/s, corresponding to droplet impact velocities of 4.1, 4.8, and 6.5 m/s, respectively. The droplet impact velocity is not linearly proportional to the variation of airflow inside the wind tunnel because the droplet is pulled more efficiently

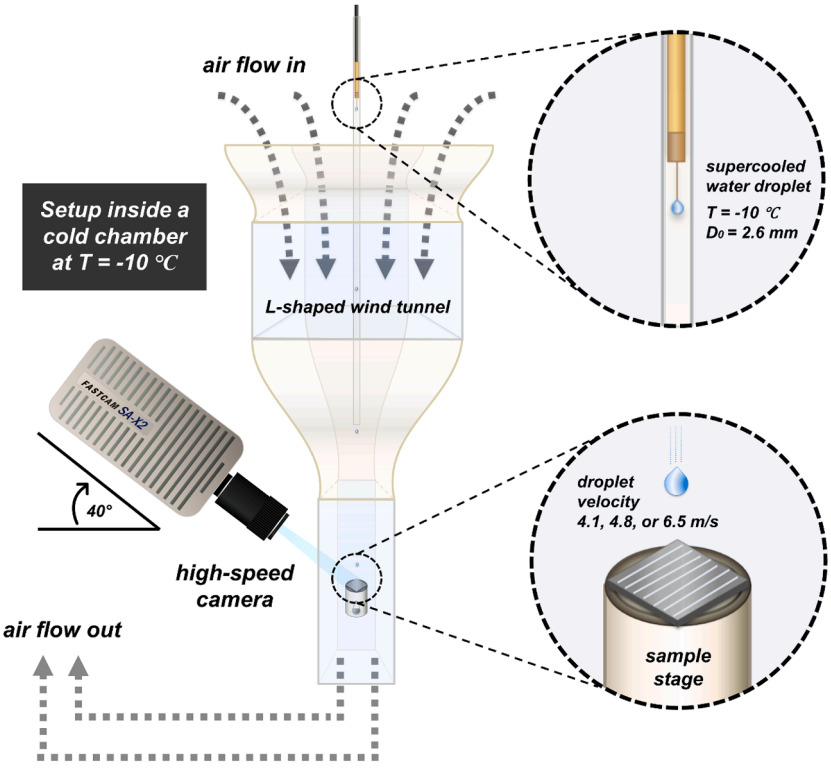

Fig. 1. A schematic presentation of the experimental setup used for the supercooled droplet impact tests.

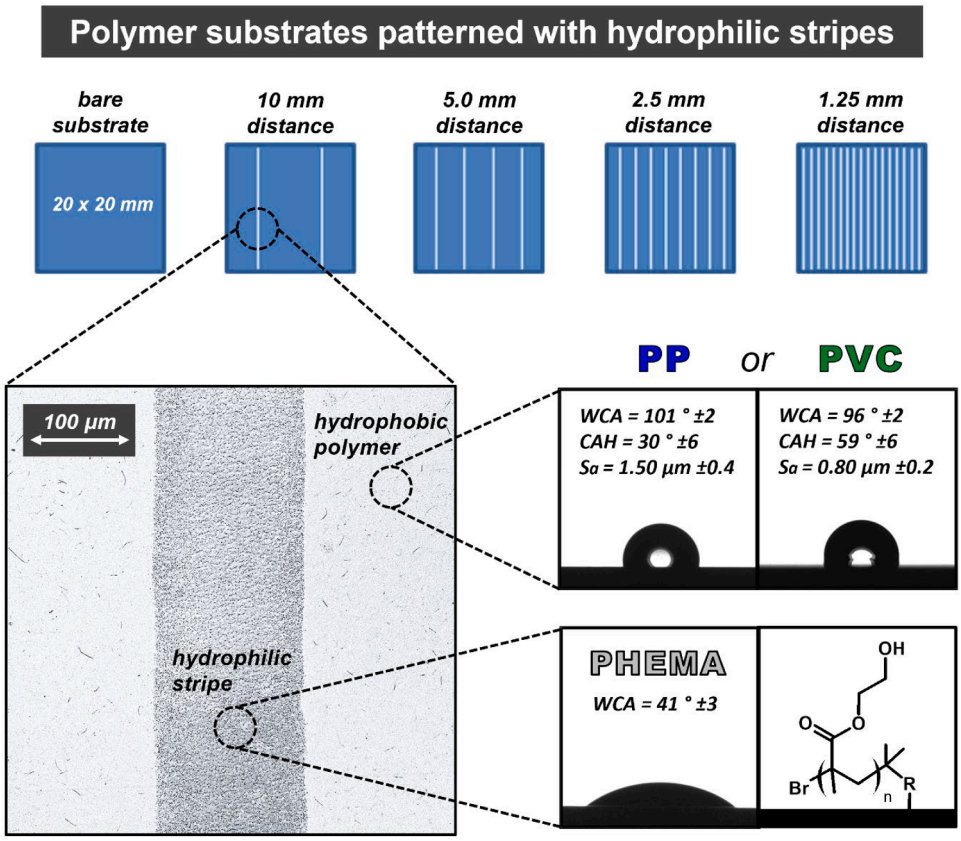

Fig. 2. The PP and PVC substrates patterned with hydrophilic PHEMA stripes were imaged using confocal microscopy (left) to determine the stripe dimensions and the substrate roughness (S_a). Static water contact angle (WCA) and contact angle hysteresis (CAH) of the bare substrates and the hydrophilic stripes were determined using contact angle goniometry (right). The chemical structure of the hydrophilic PHEMA brushes can be seen in the bottom right corner.

toward the airflow at high wind speeds. At low wind speeds, the incremental benefit is small because the drop is still mostly gravity-driven.

Figs. 3 and S2-S7 show time snapshots from four example videos, including droplet impact at a velocity of 6.5 m/s on both bare substrates (PP and PVC) and the same substrates patterned with PHEMA stripes (1.25 mm stripe distance). For each sample, the first image at $t = -1$ ms shows the square-shaped sample on the round stage holder and the falling supercooled droplet just above the sample. The second image at $t = 0.3$ ms shows the initial impact of the droplet, followed by an impact to represent droplet spread at $t = 1$ ms, and the receding process of the droplet at $t = 30$ ms. The fifth snapshot, at $t = 150$ ms, visualizes a high degree of receding (approximately maximum receding before freezing),

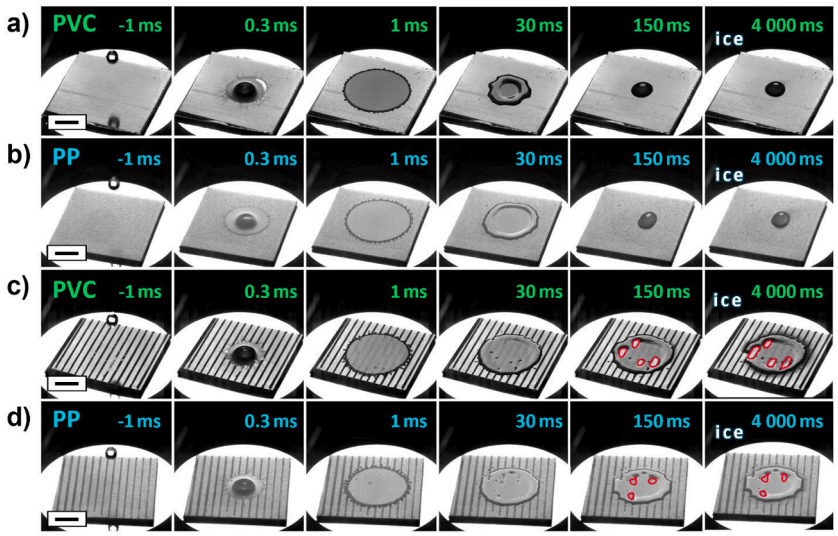

Fig. 3. A series of high-speed video snapshots showing supercooled droplet impacting, receding, and freezing stages on a) bare PVC, b) bare PP, c) patterned PVC with 1.25 mm stripe distance, and d) patterned PP with 1.25 mm stripe distance. The marked red areas highlight dry voids between the hydrophilic stripes on the patterned surfaces. All four videos were conducted under isothermal conditions at −10 °C with a droplet impact velocity of 6.5 m/s. The black scale bars at the bottom left corners correspond to 5 mm.

while the last snapshot at $t = 4000$ ms shows frozen droplets. The exact time at which each transition takes place depends on the droplet, substrate, and test as discussed here.

The droplet impact tests were repeated a minimum of 10 times for each substrate and airflow speed combination. An image processing program (ImageJ) was used to determine droplet spreading rates, freezing onset times, and freezing propagation rates from the recorded videos. For the quantification of the droplet spreading after impact, the dimensionless diameter β (t) of the droplet spread on the surface and the dimensionless time τ, defined as follows, were used:

$$\beta(t) = \frac{D(t)}{D_0} \tag{2}$$

$$\tau = t\frac{U_0}{D_0} \tag{3}$$

where D (t) is the spreading diameter, D_0 is the initial diameter of the droplet, and U_0 is the impact velocity of the droplet.

In Fig. 4, the dimensionless diameter β (t) is plotted as a function of the time after droplet impact for all PP and PVC samples in two different droplet impact velocities. In all four plots, the dimensionless diameter β (t) increases rapidly after droplet impact until it reaches its maximum spreading between $\tau = 2$–3. After maximum spreading, the wetting area recedes at a slower pace than it spreads until an equilibrium static contact angle is reached and/or the droplet begins to freeze. This holds true for all dark blue and dark green plots corresponding to bare PP and PVC (β decreases with τ after reaching a maximum). Opposite to this trend, and unlike common droplet behaviour in homogeneous samples, the spreading diameter remains steady after reaching maximum spread for all striped samples at all droplet impact velocities (β remains constant with τ after reaching a maximum). Additionally, at the lowest droplet impact velocity of 4.1 m/s (zoomed-in section in Figs. 4a-b and S8), the maximum spreading diameter of the droplet decreases with the increasing number of hydrophilic stripes.

The behaviour observed for the striped samples can be explained by the droplet being pinned as it comes in contact with the hydrophilic stripes when spreading on the surface. If the droplet covers 10 hydrophilic stripes in the moment of maximum spreading, it will remain

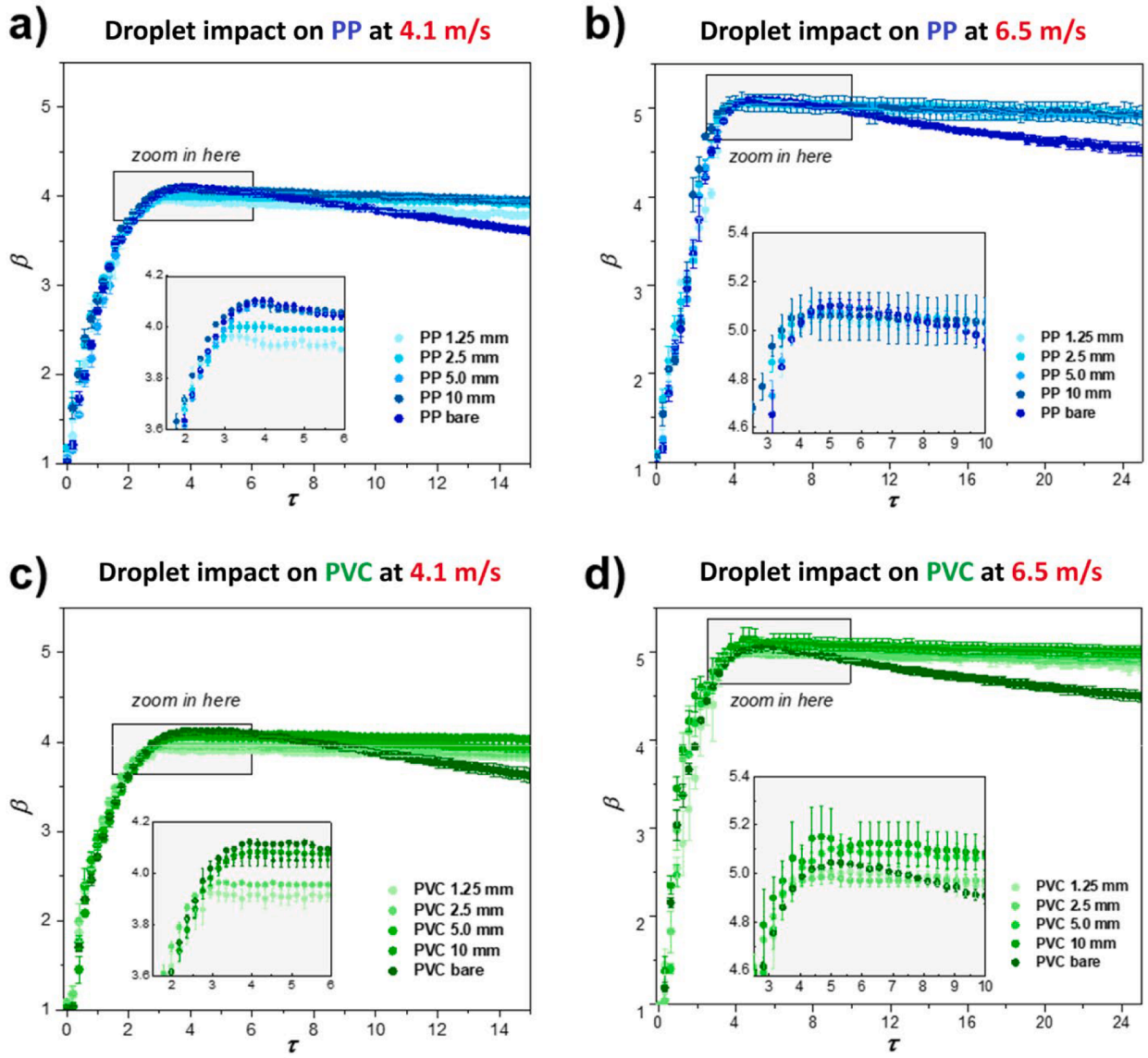

Fig. 4. The dimensionless droplet spreading diameter scaled by original droplet diameter β is plotted as a function of dimensionless time τ after droplet impact for: a) PP substrate at 4.1 m/s impact velocity; b) PP substrate at 6.5 m/s impact velocity; c) PVC substrate at 4.1 m/s impact velocity; and d) PVC substrate at 6.5 m/s impact velocity with and without stripes.

wetting these 10 stripes while receding slowly on the hydrophobic areas. Since the image analysis aims to calculate the evolution of the droplet diameter over time, rather than the overall wetted area, the dimensionless β values in Fig. 4 remain constant after the maximum droplet spreading on the patterned surfaces. This is in good agreement with previously conducted numerical simulations for patterned surfaces [24–27], in which the droplet is simultaneously wetting the hydrophilic stripes and slowly dewetting the hydrophobic polymer substrate.

At the highest impact velocity (6.5 m/s), the dewetting occasionally results in dry areas between the stripes, as shown in Figs. 3c and d It is argued that during the dry void formation, bubbles form in both hydrophilic and hydrophobic regions due to air entrainment during impact. However, hydrophilic stripes, with higher wettability and strong pinning forces, anchor the contact line, causing localized lamella thinning and rupture to be more likely. Once initiated at the hydrophilic strips, the rupture propagates into hydrophobic regions due to their lower adhesion and faster water recession. Hydrophobic areas, therefore, amplify rupture through accelerated liquid withdrawal, exposing larger dry voids.

To study this local dewetting better, a close-up analysis is needed. Fig. 5a shows representative screenshots of frozen droplets on the patterned surfaces with dry voids indicated with red circles. Although the droplets froze before the water fully receded from the hydrophobic areas, the occasional dry voids between the stripes suggest that the patterning directs the final water distribution. Fig. 5b presents the sum of all detected void areas per sample for quantitative assessment of each sample's void formation tendency at a given speed of 6.5 m/s (i.e. dewetted area added together from all the impacts for a specific speed and substrate). This approach is selected as it is closer to a real-life icing scenario where multiple supercooled droplets impact a larger area.

Since the void formation was observed only at the highest impact velocity (6.5 m/s), the probability of void formation is expected to increase with increasing droplet impact velocity. Fig. 5b also shows that the probability of void formation seems to increase with decreasing stripe distance, with the PP substrate showing more void areas than the PVC samples. This is likely due to the combination of lower wettability and slightly higher roughness of the PP substrate. By increasing droplet impact velocity and by maximizing the wetting contrast between the stripes and the substrate (i.e., stripes with a lower static contact angle on a substrate with a higher static contact angle), the impacted droplet would recede faster towards the hydrophilic patterns and the final shape of the frozen area would mimic the predetermined surface patterning.

3.3. Influence of hydrophilic patterns on droplet freezing after impact

Ice nucleation can occur anytime after droplet impact; however, high-speed videos from longer than 18 s of recording time result in unreasonably large video files that cannot be produced and stored in large quantities. As a consequence of this technical limitation and the long freezing times observed in some experiments, some droplet freezing were not recorded.

Fig. 6 shows the freezing probabilities for each sample with the three different droplet impact velocities. As expected, the droplet freezing probabilities increase with higher impact velocities due to more small air bubbles generated at the liquid-solid interface during impact [20]. On the other hand, the samples with PVC substrate show higher freezing probabilities even though Fig. 2 shows that the PP substrates have slightly higher roughness (S_a = 1.50 μm > 0.80 μm). Since these experiments were conducted in isothermal conditions, differences in thermal conductivities (0.12 W/mK for PP and 0.19 W/mK for PVC) [30], are unlikely to account for the higher freezing probability of PVC. On the other hand, the higher wettability of PVC compared to PP (Fig. 2 showing CAH values 59°>30°) likely leads to more continuous molecular water layers on PVC, which have in turn been proven to promote earlier freezing onset times in surface frosting [31] and could be the underlying reason for more rapid droplet freezing observed in this work. An existing layer of interfacial ice-like water, which has previously been identified and described even on surfaces modified with hydrophobic alkyl silanes and halocarbon wax [32], provides thermodynamically ideal hydrophilic surfaces for nucleation events [33]. The presence of these hydrophilic MWLs promote earlier nucleation on the PVC substrate, leading to higher freezing probability in the supercooled droplet impact tests.

The surface coverage of each frozen droplet was analyzed from the recorded videos using ImageJ and plotted as a function of the nucleation onset time after droplet impact. In Fig. 7a, the frozen droplet areas decrease exponentially with increasing time after the droplet impact. After $t = 1$ s, the frozen area coverage remains below 40 mm^2 (less than a third of the maximum droplet spreading ~150 mm^2) regardless of the substrate type or droplet impact velocity. As mentioned earlier, complete receding of the droplet before freezing onset is necessary for controlling the shape of the frozen area with better precision. Therefore, the freezing onset time for these samples should ideally be higher than one second.

Since freezing after droplet impact is a stochastic process, reporting average freezing onset times for each sample is irrelevant in this context. Instead, the freezing onset times for each sample were plotted as the

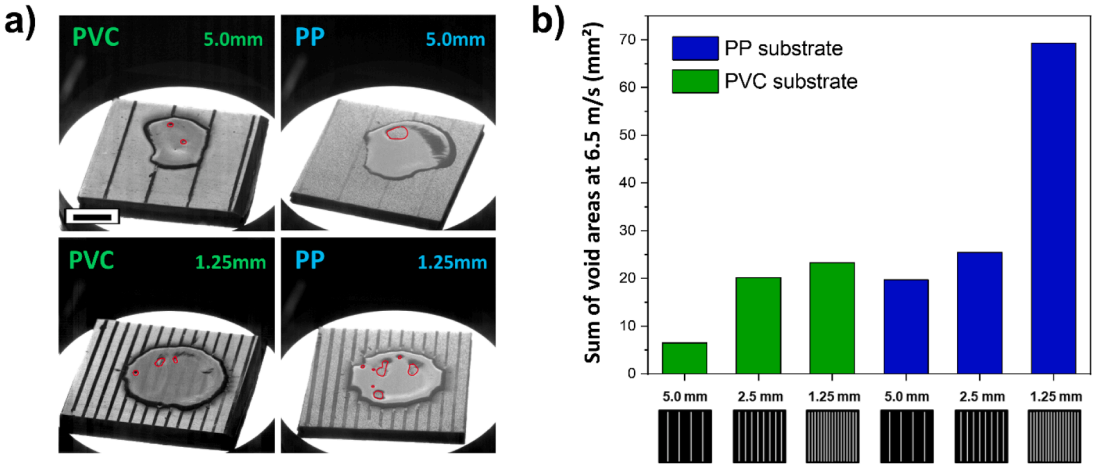

Fig. 5. a) Video snapshots showing regions of dry voids (circled with a red line) on PVC and PP substrates with 5.0 mm and 1.25 mm stripe distance impacted at 6.5 m/s. The black scale bar on the bottom left corner of the first image corresponds to 5 mm. b) Sum of all detected void areas on the patterned PVC and PP substrates with varying distances between the hydrophilic stripes at 6.5 m/s impact velocity.

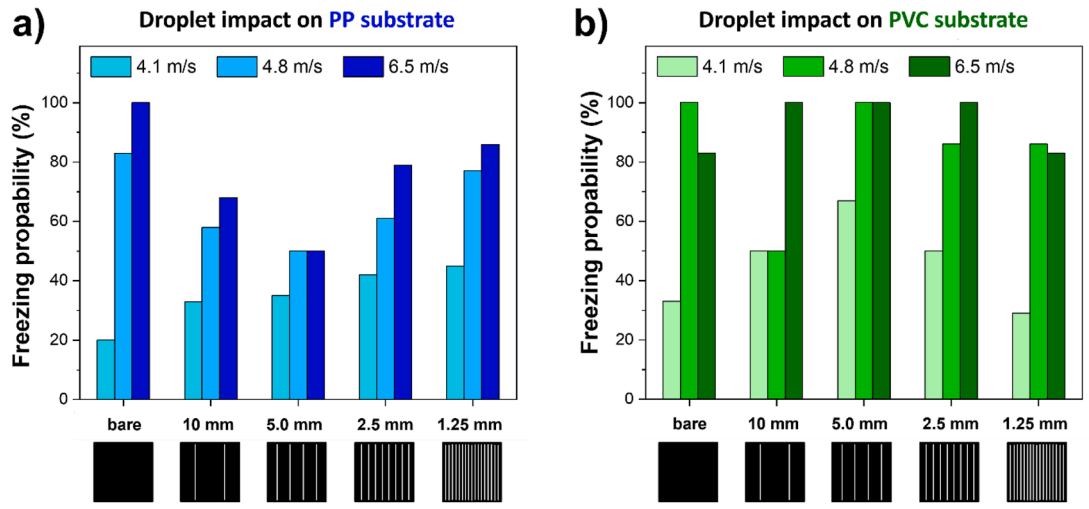

Fig. 6. Freezing probabilities with a droplet impact velocity of 4.1 m/s, 4.8 m/s, and 6.5 m/s for the various patterned samples with a) a PP substrate (blue color) or b) a PVC substrate (green color).

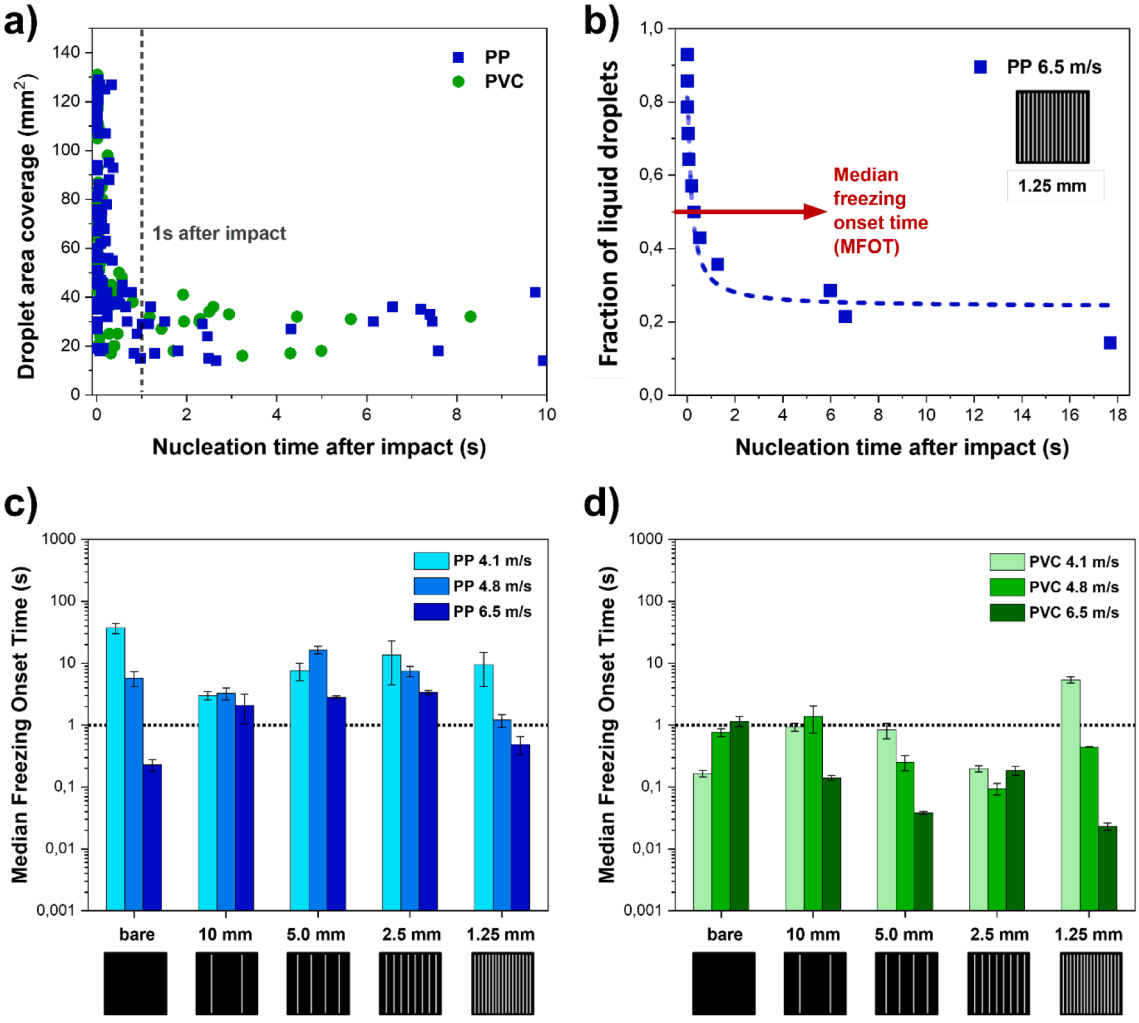

Fig. 7. a) The surface coverage of each frozen droplet plotted as a function of droplet nucleation time after impact. b) Fraction of liquid droplets plotted as a function of all nucleation onset times of droplets impacting a PP substrate with 1.25 mm stripe distance at a velocity of 6.5 m/s. The nucleation onset time corresponding to the half point of frozen and liquid droplets (red arrow) is denoted as the median freezing onset time (MFOT). The MFOTs are shown for all samples with c) PP substrate (blue) and d) PVC substrate (green). The dotted black line indicates $t = 1$ s after the impact.

fraction of liquid droplets Q_{liq}(t) at the given onset time after the droplet impact.

$$Q_{liq}(t) = \frac{N_{liq}(t)}{N_0} \quad (4)$$

As shown in Fig. 7b, the resulting plot shows the fraction of liquid droplets freezing at longer times decays exponentially. By fitting an exponential power function to this plot, it is possible to extract the theoretical time after droplet impact at which there is a 50 % chance that the droplet has already frozen. This parameter will be denoted as the median freezing onset time (MFOT). The MFOTs for each sample with the three different droplet impact velocities are shown in Fig. 7c-d. Similarly to the freezing probabilities in Fig. 6, the MFOTs are significantly higher for droplet impact on PP substrates, and decrease with increasing droplet impact velocity for most samples. The MFOTs on PP substrate are also mostly above 1 s, indicating that the droplets impacting PP substrate have more time to recede and form larger dry voids than droplets impacting PVC substrate before they freeze.

In addition to the freezing probabilities and MFOTs, the droplet areas at freezing onset times $A_c(t)$ and the fraction of liquid droplets $N_{liq}(t)/N_0$ were used to calculate the average number of nucleation sites $\lambda_s(t)$ and average nucleation rates per unit area $J_s(t)$ for each sample, as shown in Eq. (1).

Fig. 8a shows examples of $\lambda_s(t)$ plotted as a function of the droplet nucleation time after impact for the patterned samples. For all samples, the $\lambda_s(t)$ values increase linearly over time, with the slope corresponding to the average nucleation rate $J_s(t)$. As shown in Fig. 8b, the initial nucleation rate at $t < 50$ ms is significantly higher compared to the second nucleation rate thereafter. The higher nucleation rate at $t < 50$ ms is attributed to the air bubbles generated at droplet impact. For droplets freezing after 50 ms, the nucleation rate decreases, attributed to the impact of trapped bubbles disappearing.

The average nucleation rates for all samples can be seen in Fig. 8c-d. As expected, the initial nucleation rates at $t < 50$ ms (Fig. 8c) are higher for all samples compared to the second nucleation rate at $t > 50$ ms (Fig. 8d); i.e., nucleation happens at higher speeds when droplets freeze within 50 ms after impact. Following the same trend of freezing probability and MFOTs, the nucleation rates are also much higher for PVC substrates (green color) than for PP (blue color), again attributed to the presence of MWL on PVC. The differences between droplet impact velocities and stripe distances are less obvious, especially at $t < 50$ ms in Fig. 8c. However, the striped PVC samples in Fig. 8d show higher nucleation rates at $t > 50$ ms compared to the bare PVC sample. An opposite trend can be seen in Fig. 8d for the striped PP samples, which show lower nucleation rates at $t > 50$ ms compared to the bare PP substrate. This reinforces the idea that the wettability difference between the substrate and the patterns should be maximised to lower nucleation rates, which increases the median freezing onset time MFOT,

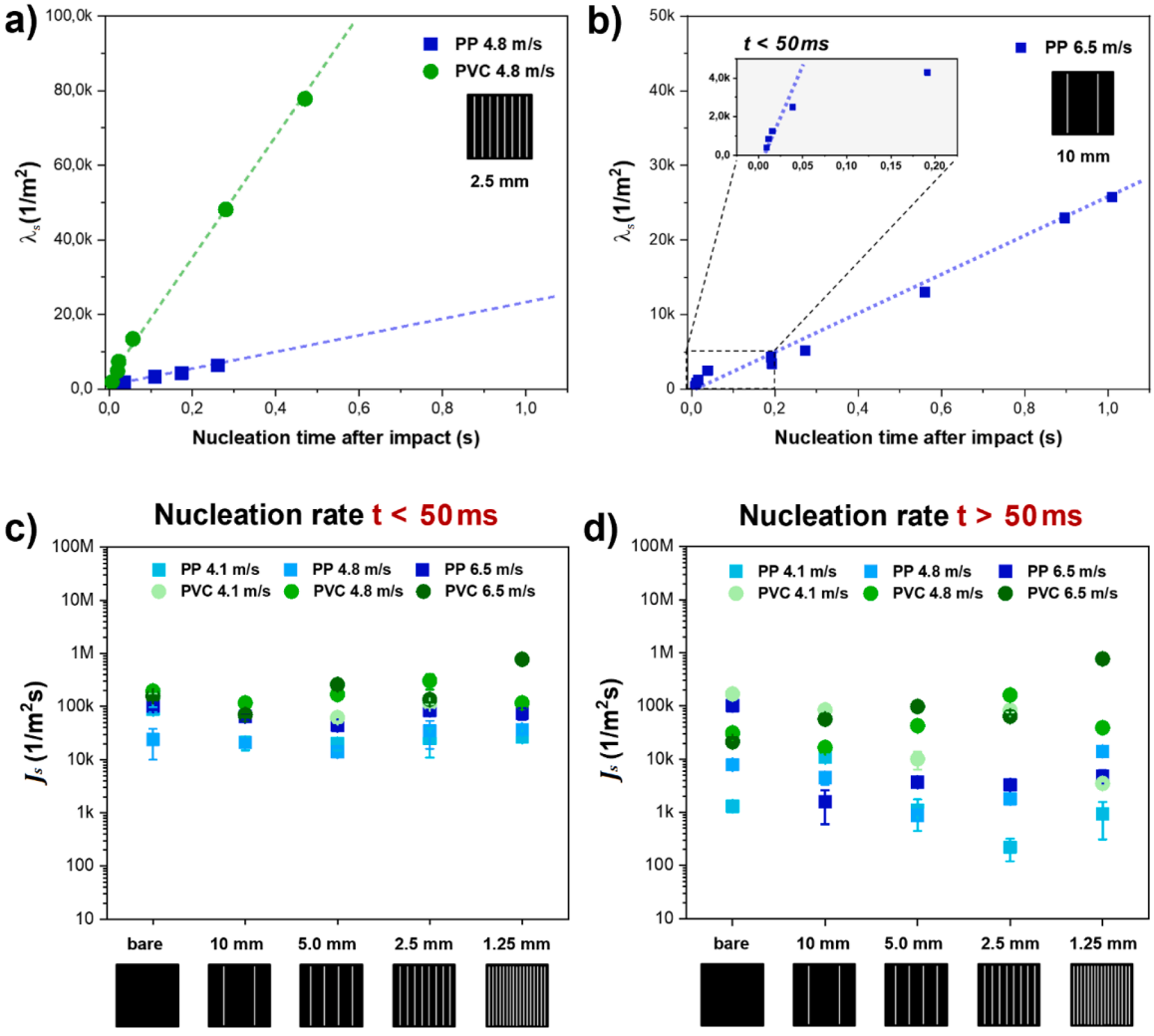

Fig. 8. Average number of nucleation sites per unit area (λ_s) as a function of the nucleation time after droplet impact for samples a) PP and PVC with 2.5 mm stripe distance and 4.8 m/s droplet velocity, and b) PP with 10 mm stripe distance and 6.5 m/s droplet velocity. From the slopes of the $\lambda_s(t)$ plots nucleation rates (J_s) for the samples at c) $t < 50$ ms and d) $t > 50$ ms can be obtained.

which, in turn, creates more time for the droplet to recede towards the hydrophilic patterning.

Once a freezing event initiates after the droplet impact, its propagation within the supercooled droplet can also be followed in the recorded videos. The rate of freezing propagation within the droplet was analyzed using ImageJ for all of the experiments, and their values were plotted in Fig. 9. All propagation rates were found to be between 50 and 100 mm/s with no variation between the two substrates, distance between the hydrophilic stripes, or droplet impact velocity. These values are comparable to those reported for bulk water freezing [31,34–36] being between 10 and 100 mm/s, as expected since the freezing propagation within the supercooled droplet is bulk water freezing, given the dimensions of the droplet. The droplet freezing mechanism after impact is therefore confirmed to be governed by bulk water freezing dynamics, independent of surface effects.

As a mode of summary of the different observations made during supercooled water droplet impact, Fig. 10 shows a comparison of the droplet wetting and freezing behaviour on the two different polymeric substrates (PP and PVC). For both substrates, dry voids were detected when the patterning distance was lower than 5 mm, with the probability of void formation increasing with decreasing stripe distance. Fig. 10a-b shows the overall average nucleation rates ($t > 50$ ms) on both substrates at all impact velocities to highlight the differences as a function of the underlying polymer substrate. Both substrates show the lowest nucleation rates for stripe distances between 2.5 and 5 mm, although the patterned PP substrates had significantly lower nucleation rates compared to the PVC samples.

Overall, the patterned PVC samples show increased nucleation rates compared to the bare PVC substrate, whereas the patterned PP samples show an opposite trend. We hypothesize that this behaviour is due to the wettability contrast between substrate and stipes (higher for PP samples), as well as the presence of MWL on PVC. Although further testing on more hydrophobic substrates with higher wettability contrast could lead to faster droplet receding and bigger dry areas, this study provides important initial insights into the performance of patterned wettability surfaces as passive anti-icing coatings in dynamic icing conditions. During in-flight icing conditions, supercooled water droplets can impact the aircraft surfaces with velocities up to 500 m/s, which is an order of magnitude higher than the impact velocities used in this work (up to 6.5 m/s). Since dry void formation was observed only at the highest impact velocity, higher droplet impact velocities in real-life icing conditions could potentially significantly increase the droplet receding rate toward the hydrophilic patterns, thus leading to better control over where ice is formed on the surface.

4. Conclusions

The impact behaviour of supercooled droplets ($D_0 = 2.6$ mm) on homogeneous and patterned wettability surfaces was investigated in an l-shaped wind tunnel at isothermal conditions of −10 °C at three different impact velocities. Two commodity polymers (PP and PVC) with different CAH (30° and 59°) were covered with hydrophilic stripes (150 μm wide PHEMA stripes) to create patterned samples with two different wettability regions. A high-speed camera was used to monitor the droplet impact on the hydrophilic stripes, with stripe distance varying from 1.25 mm to 10 mm, and the droplet impact velocities adjusted at 4.1, 4.8, and 6.5 m/s.

The captured high-speed videos show occasional dry voids between the hydrophilic stripes during the receding of impacted supercooled droplets at the highest impact velocity (6.5 m/s). Image analysis of the frozen droplets reveals that the void formation is more likely to occur with a higher wettability difference (PP substrate) and with a lower patterning distance. The higher wettability difference on PP was also linked to a reduced nucleation probability and rate after droplet impact. Even though the freezing onset occurs on both substrates before the droplet has fully receded towards the hydrophilic stripes, the numerous dry voids on PP suggest that an even higher wettability difference between the hydrophilic patterns and the hydrophobic substrate could help control the shape and location of the final frozen area after droplet impact.

Unlike the patterned PVC substrates, the hydrophilic patterning on PP leads to overall better performance in terms of nucleation rates and wetting behavior compared to bare PP. Specifically, PP samples with a patterning distance of 2.5–5.0 mm exhibit the lowest freezing probabilities and nucleation rates under the experimental conditions used in this work (a droplet diameter of 2.6 mm, impact velocities of 4.1–6.5 m/s, and an isothermal temperature of −10 °C). While lower freezing probability is more critical for anti-icing surfaces from a practical point of view, freezing onset time after impact can play a crucial role in the aim of controlling where and in what shape ice accumulates on patterned surfaces. The later the freezing onset occurs, the more time the droplet has to recede towards the hydrophilic patterning, thus generating dry areas that grow between the patterns.

This work is first experimental study that investigates systematically the influence of wettability patterns on supercooled water droplet impact, wetting, and freezing behaviour. The results indicate that patterned wettability surfaces could be potentially beneficial under impact icing conditions, especially when considering the higher impact velocities and using a lower patterning distance that can aid in faster and

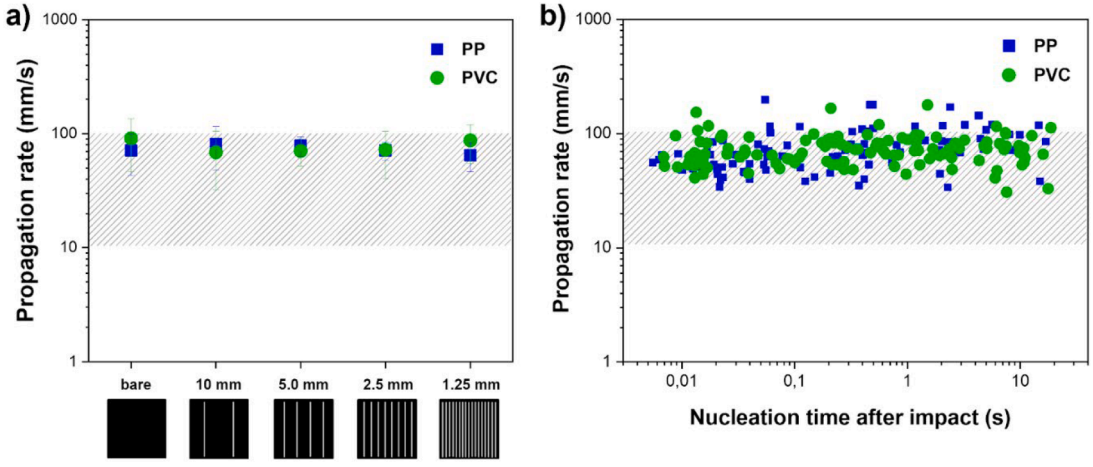

Fig. 9. Freezing propagation rate within the droplet after impact for all of the patterned PP (blue) and PVC (green) samples and all droplet velocities as a function of a) the distance between the hydrophilic stripes; b) the nucleation time after impact. The gray dashed grid indicates the range of propagation rates previously reported for bulk water freezing [31,34–36].

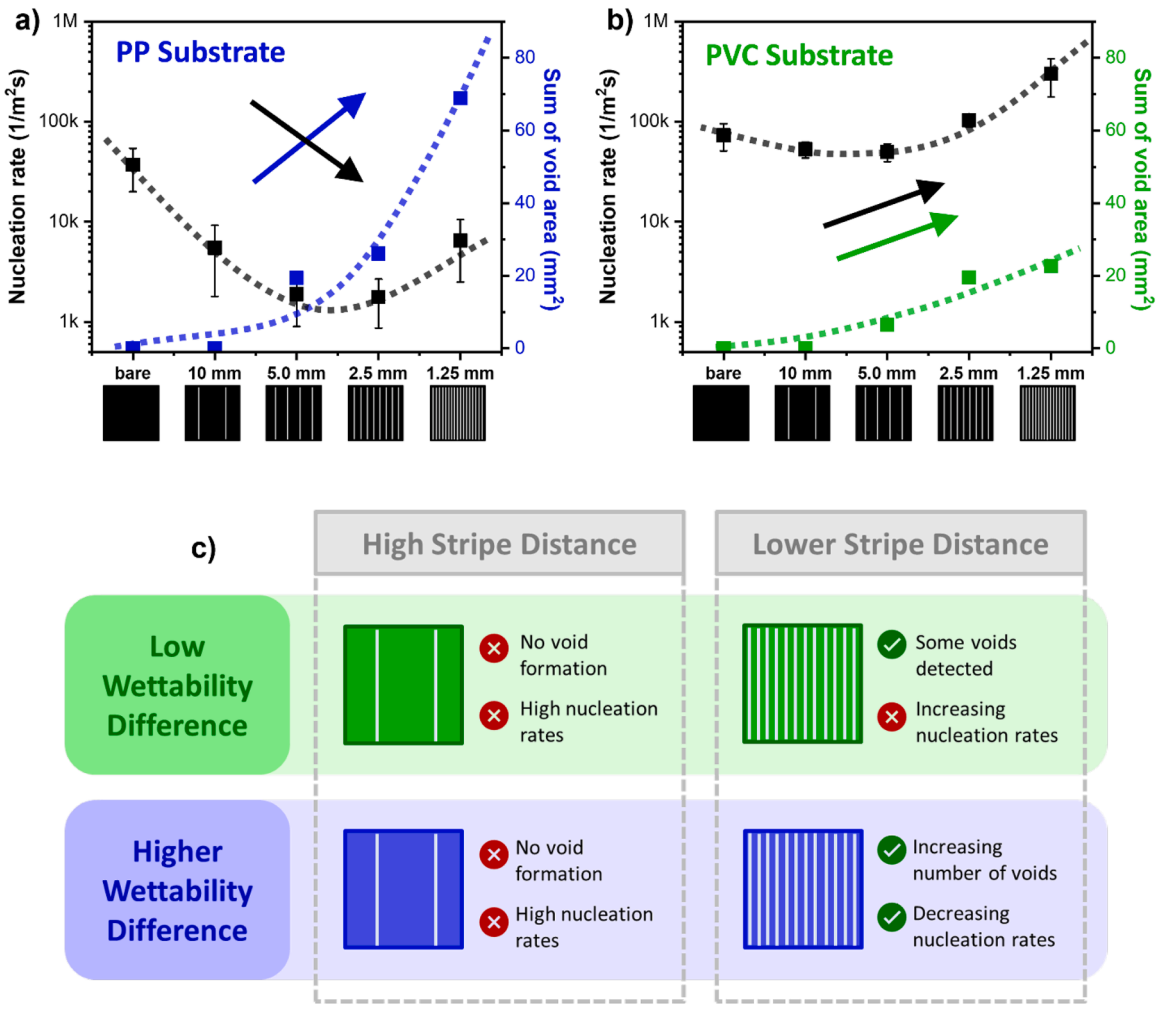

Fig. 10. Average nucleation rates ($t > 50$ ms) and the dry void areas as a function of the stripe density for samples with a) PP substrate (blue) and b) PVC substrate (green). The dotted lines are a guide for the eye. c) Summary of the trends seen in plots a) and b).

more frequent dry void formation. Although the droplet impact velocities used in this study (4.1–6.5 m/s) are much lower than what anti-icing coatings would experience in potential real-life applications (e.g. supercooled droplet impact on aircraft at 50–500 m/s), the dry void formation in the highest tested impact velocity is an encouraging sign for further systematic tests in more challenging environmental conditions. Finally, to develop rational designs for future patterned anti-icing surfaces, a more in-depth investigation is needed into the role of patterning distance, shape, chemistry, and topology on the freezing of impacting supercooled droplets, particularly in connection with varying droplet diameter and impact velocity.

CRediT authorship contribution statement

M.J. Tavaststjerna: Writing – original draft, Visualization, Investigation, Formal analysis, Data curation. **M. Ding:** Writing – review & editing, Validation, Project administration, Methodology, Investigation, Formal analysis, Data curation. **J. Hussong:** Writing – review & editing, Supervision. **S.J. Picken:** Writing – review & editing, Supervision. **I.V. Roisman:** Writing – review & editing, Supervision, Methodology, Funding acquisition, Formal analysis. **S.J. Garcia:** Writing – review & editing, Supervision, Funding acquisition, Formal analysis, Conceptualization.

Declaration of competing interest

The authors declare that they have no known competing financial interests or personal relationships that could have appeared to influence the work reported in this paper.

Acknowledgments

This project has received funding from the European Union's Horizon 2020 research programme under the Marie Skłodowska-Curie grant agreement No 956703 (SURFICE project).

Supplementary materials

Supplementary material associated with this article can be found, in the online version, at doi:10.1016/j.surfin.2025.107918.

Data availability

Data will be made available on request.

References

[1] Y. Cao, W. Tan, Z. Wu, Aircraft icing: an ongoing threat to aviation safety, Aerosp. Sci. Technol. 75 (2018) 353–385, https://doi.org/10.1016/j.ast.2017.12.028.

[2] M. Yamazaki, A. Jemcov, H. Sakaue, A review on the current status of icing physics and mitigation in aviation, Aerospace 8 (2021), https://doi.org/10.3390/aerospace8070188.
[3] X. Huang, N. Tepylo, V. Pommier-Budinger, M. Budinger, E. Bonaccurso, P. Villedieu, L. Bennani, A survey of icephobic coatings and their potential use in a hybrid coating/active ice protection system for aerospace applications, Prog. Aerospace Sci. 105 (2019) 74–97, https://doi.org/10.1016/j.paerosci.2019.01.002.
[4] P. Irajizad, S. Nazifi, H. Ghasemi, Icephobic surfaces: definition and figures of merit, Adv. Colloid Interface Sci. 269 (2019) 203–218, https://doi.org/10.1016/j.cis.2019.04.005.
[5] F. Wang, Y. Zhuo, Z. He, S. Xiao, J. He, Z. Zhang, Dynamic Anti-Icing Surfaces (DAIS), Advanc. Sci. 8 (2021) 2101163, https://doi.org/10.1002/advs.202101163.
[6] Y. Shen, X. Wu, J. Tao, C. Zhu, Y. Lai, Z. Chen, Icephobic materials: fundamentals, performance evaluation, and applications, Prog. Mater. Sci. 103 (2019) 509–557, https://doi.org/10.1016/j.pmatsci.2019.03.004.
[7] M. Susoff, K. Siegmann, C. Pfaffenroth, M. Hirayama, Evaluation of icephobic coatings—Screening of different coatings and influence of roughness, Appl. Surf. Sci. 282 (2013) 870–879, https://doi.org/10.1016/j.apsusc.2013.06.073.
[8] S. Peppou-Chapman, J.K. Hong, A. Waterhouse, C. Neto, Life and death of liquid-infused surfaces: a review on the choice, analysis and fate of the infused liquid layer, Chem. Soc. Rev. 49 (2020) 3688–3715, https://doi.org/10.1039/D0CS00036A.
[9] S. Jung, M. Dorrestijn, D. Raps, A. Das, C.M. Megaridis, D. Poulikakos, Are superhydrophobic surfaces best for icephobicity? Langmuir 27 (2011) 3059–3066, https://doi.org/10.1021/la104762g.
[10] J. Chen, J. Liu, M. He, K. Li, D. Cui, Q. Zhang, X. Zeng, Y. Zhang, J. Wang, Y. Song, Superhydrophobic surfaces cannot reduce ice adhesion, Appl. Phys. Lett. 101 (2012), https://doi.org/10.1063/1.4752436.
[11] S.A. Kulinich, S. Farhadi, K. Nose, X.W. Du, Superhydrophobic surfaces: are they really ice-repellent? Langmuir 27 (2011) 25–29, https://doi.org/10.1021/la104277q.
[12] H.Y. Erbil, Practical Applications of Superhydrophobic Materials and Coatings: problems and Perspectives, Langmuir 36 (2020) 2493–2509, https://doi.org/10.1021/acs.langmuir.9b03908.
[13] J.L. O'Brien, S.F. Ahmadi, K.C. Failor, C.E. Bisbano, M.D. Mulroe, S. Nath, B. A. Vinatzer, J.B. Boreyko, Spatial control of condensation and desublimation using ice nucleating proteins, Appl. Phys. Lett. 113 (2018), https://doi.org/10.1063/1.5046187.
[14] Y. Jin, C. Wu, Y. Yang, J. Wu, Z. He, J. Wang, Inhibiting Condensation Freezing on Patterned Polyelectrolyte Coatings, ACS Nano. 14 (2020) 5000–5007, https://doi.org/10.1021/acsnano.0c01304.
[15] M.J. Tavaststjerna, S.J. Picken, S.J. Garcia, Controlling Frost Propagation on Polymeric Surfaces Using SI-ATRP Chemical Micropatterning, Adv. Mater. Interfaces N/A. (2025) 2400838, https://doi.org/10.1002/admi.202400838.
[16] X. Zhou, Y. Sun, J. Liu, Designing Anti-Icing Surfaces by Controlling Ice Formation, Adv. Mater. Interface. 8 (2021), https://doi.org/10.1002/admi.202100327.
[17] S.M. Mousavi, F. Sotoudeh, B. Chun, B.J. Lee, N. Karimi, S.A. Faroughi, The potential for anti-icing wing and aircraft applications of mixed-wettability surfaces - A comprehensive review, Cold. Reg. Sci. Technol. 217 (2024), https://doi.org/10.1016/j.coldregions.2023.104042.
[18] X. Zhang, X. Liu, X. Wu, J. Min, Impacting-freezing dynamics of a supercooled water droplet on a cold surface: rebound and adhesion, Int. J. Heat Mass Transf. 158 (2020), https://doi.org/10.1016/j.ijheatmasstransfer.2020.119997.
[19] C. Tang, M. Qin, X. Weng, X. Zhang, P. Zhang, J. Li, Z. Huang, Dynamics of droplet impact on solid surface with different roughness, Int. J. Multiphase Flow. 96 (2017) 56–69, https://doi.org/10.1016/j.ijmultiphaseflow.2017.07.002.
[20] M. Ding, J. Hussong, I.V. Roisman, Freezing of a Supercooled Water Drop after an Impact onto a Solid Wall, Cold. Reg. Sci. Technol. 229 (2024).
[21] M. Sun, W. Kong, F. Wang, H. Liu, Impact freezing modes of supercooled droplets determined by both nucleation and icing evolution, Int. J. Heat Mass. Transf. 142 (2019), https://doi.org/10.1016/j.ijheatmasstransfer.2019.07.081.
[22] M. Schremb, I. Roisman, C. Tropea, Transient effects in ice nucleation of a water drop impacting onto a cold substrate, Phys. Rev. E. 95 (2017) 022805.
[23] H. Wu, W. Kong, P. Bian, H. Liu, The coupled impact-freezing mechanism of supercooled droplet on superhydrophobic surface, Aerospace Syst. 7 (2024) 11–28, https://doi.org/10.1007/s42401-023-00192-y.
[24] T. Pravinraj, R. Patrikar, A droplet actuation technique for a lab-on-chip device using partial wetting surface without external force, Sens. Actuator. A Phys. 285 (2019) 482–490, https://doi.org/10.1016/j.sna.2018.11.039.
[25] J. Göhl, A. Mark, S. Sasic, F. Edelvik, An immersed boundary based dynamic contact angle framework for handling complex surfaces of mixed wettabilities, Int. J. Multiphase Flow. 109 (2018) 164–177, https://doi.org/10.1016/j.ijmultiphaseflow.2018.08.001.
[26] Z. Yuan, M. Matsumoto, R. Kurose, Directional migration of an impinging droplet on a surface with wettability difference, Phys. Rev. Fluid. 5 (2020), https://doi.org/10.1103/PhysRevFluids.5.113605.
[27] J. Huang, L. Wang, K. He, Three-dimensional study of double droplets impact on a wettability-patterned surface, Comput. Fluid. 248 (2022), https://doi.org/10.1016/j.compfluid.2022.105669.
[28] F. Sotoudeh, R. Kamali, S.M. Mousavi, N. Karimi, B.J. Lee, D. Khojasteh, Understanding droplet collision with superhydrophobic-hydrophobic–hydrophilic hybrid surfaces, Colloid. Surf A. Physicochem. Eng. Asp. 614 (2021), https://doi.org/10.1016/j.colsurfa.2021.126140.
[29] A. Russo, M. Icardi, M. Elsharkawy, D. Ceglia, P. Asinari, C.M. Megaridis, Numerical simulation of droplet impact on wettability-patterned surfaces, Phys. Rev. Fluid. 5 (2020), https://doi.org/10.1103/PhysRevFluids.5.074002.
[30] I.-L. Ngo, S. Jeon, C. Byon, Thermal conductivity of transparent and flexible polymers containing fillers: a literature review, Int. J. Heat Mass Transf. 98 (2016) 219–226, https://doi.org/10.1016/j.ijheatmasstransfer.2016.02.082.
[31] M.J. Tavaststjerna, S.J. Picken, S.J. Garcia, Role of Molecular Water Layer State on Freezing Front Propagation Rate and Mode Studied with Thermal Imaging, Langmuir 40 (2024) 12888–12898, https://doi.org/10.1021/acs.langmuir.4c00323.
[32] A.L. Sumner, E.J. Menke, Y. Dubowski, J.T. Newberg, R.M. Penner, J. C. Hemminger, L.M. Wingen, T. Brauers, B.J. Finlayson-Pitts, The nature of water on surfaces of laboratory systems and implications for heterogeneous chemistry in the troposphere, Physic. Chem. Chemic. Phys. 6 (2004) 604–613, https://doi.org/10.1039/B308125G.
[33] S. Nath, J.B. Boreyko, On Localized Vapor Pressure Gradients Governing Condensation and Frost Phenomena, Langmuir 32 (2016) 8350–8365, https://doi.org/10.1021/acs.langmuir.6b01488.
[34] J.E. Castillo, Y. Huang, Z. Pan, J.A. Weibel, Quantifying the Pathways of Latent Heat Dissipation during Droplet Freezing on Cooled Substrates, Int. J. Heat Mass Transf. 164 (2021) 120608, https://doi.org/10.1016/j.ijheatmasstransfer.2020.120608.
[35] Z. Meng, P. Zhang, Dynamic propagation of ice-water phase front in a supercooled water droplet, Int. J. Heat Mass Transf. 152 (2020), https://doi.org/10.1016/j.ijheatmasstransfer.2020.119468.
[36] M. Schremb, I.V. Roisman, C. Tropea, Normal impact of supercooled water drops onto a smooth ice surface: experiments and modelling, J. Fluid. Mech. 835 (2018) 1087–1107, https://doi.org/10.1017/jfm.2017.797.